Cancer Chemother Pharmacol (1997) 40: 101–111

ORIGINAL ARTICLE

Kevin K. Millis · Stephen A. Lesko · Michael P. Gamcsik

Formation, Intracellular distribution and efflux of glutathione–bimane conjugates in drug-sensitive and -resistant MCF-7 cells

Received: 9 May 1996 / Accepted: 19 November 1996

Abstract The rate of reaction of monochlorobimane with glutathione (GSH) was measured in native human mammary MCF-7 adenocarcinoma cells (MCF-7wt) and sublines displaying resistance to 4-hydroperoxycyclophosphamide (MCF-7hc) and adriamycin (MCF-7adr) prior to examination by epifluorescence and confocal microscopy. After a 60-min incubation period at 37 °C, essentially all GSH was conjugated in the MCF-7wt and MCF-7adr cell lines whereas only 80% of the GSH was conjugated in the MCF-7hc line. All three lines displayed significant export of the conjugate from the cell during this period, with the MCF-7adr line displaying the most rapid efflux with 85% of the conjugate exported within 60 min. Epifluorescence microscopy detected an approximately 20% increase in integrated fluorescence intensity in the nuclear region in all three lines. Confocal microscopy however, indicated that most of the cells examined showed a homogeneous fluorescence distribution. The cells grown in monolayers were found to be thicker in the nuclear region suggesting that the observed increase in fluorescence intensity in the nuclear region in the images from epifluorescence microscopy was probably derived from fluorescence from an out-of-focus plane. Cells depleted of GSH with buthionine sulfoximine followed by treatment with mBCl showed significant fluorescence intensity resulting from nonspecific binding of this probe. These studies illustrate the need for measuring the rate of GSH conjugate export and for determining probe specificity, and emphasizes the need for using confocal techniques for the quantitative evaluation of the distribution of intracellular fluorescence.

Key words Microscopy · Monochlorobimane · Epifluorescence · Confocal · Glutathione-S-transferase

Abbreviations *GSH* glutathione · *GSSG* oxidized glutathione disulfide · *BSO* buthionine sulfoximine · *mBCl* monochlorobimane · *mBBr* monobromobimane · *MCB-GSH* bimane–glutathione conjugate · *GST* glutathione-S-transferase · f_{nuc}/f_{cyt} nuclear-to-cytoplasmic fluorescence intensity ratio · *MEM* Eagle's minimal essential medium · *FBS* fetal bovine serum · *HBSS* Hanks' balanced salt solution · *MRP* multidrug resistance protein

Introduction

Glutathione (GSH) appears to play an important role in the ability of cancer cells to resist the cytotoxic effects of chemotherapeutic drugs and radiation [29, 36, 44, 47, 48]. In some cell lines, depletion of GSH by buthionine sulfoximine (BSO) [21] treatment has been shown to increase the efficacy of drug and/or radiation treatment [33, 42, 43]. Previous studies of mitochondria [25, 35] and isolated nuclei [8, 15, 16, 24, 53] suggest the existence of distinct subcellular pools of GSH. This compartmentalization of GSH may be important in evaluating cellular response to therapy especially if certain regions of the cell exhibit significantly increased GSH levels. This is particularly important since differences between the nuclear and cytoplasmic distribution of drugs such as doxorubicin correlate with resistance [30]. Information on the subcellular distribution of GSH, however, is not obtainable from conventional biochemical assays which use cell lysates.

K.K. Millis · M.P. Gamcsik[1] (✉)
Department of Radiology,
Johns Hopkins University School of Medicine,
Baltimore, MD 21205, USA

S.A. Lesko
Department of Biochemistry,
School of Hygiene and Public Health,
Johns Hopkins University,
Baltimore, MD 21205, USA

Current address:
[1]Duke University Medical Center,
Box 3843 Durham, NC 27710, USA
Tel. (919) 681 2244; Fax (919) 684 5633

Epifluorescence and confocal fluorescence microscopy techniques are nondestructive and, in conjunction with image analysis, can be used to construct three-dimensional maps of fluorescence intensity in living cells. Since the optimal resolution is adequate to distinguish nuclear from cytosolic regions, we used these techniques to visualize the intracellular distribution of fluorescent GSH conjugates in living breast cancer cells.

Several fluorescent probes for GSH are currently available and include mercury orange [3, 31, 39], *o*-phthaldialdehyde [54], chloromethyl fluorescein diacetate [45], monobromobimane (mBBr) [26] and monochlorobimane (mBCl) [28, 46]. To date, mBCl is reported to be the most specific probe because its conjugation with GSH to form the highly fluorescent bimane–glutathione (MCB-GSH) adduct is catalyzed by endogenous glutathione S-transferase (GST) isozymes [12, 55]. The efficiency of this catalysis is isozyme dependent, with the μ and π isozyme classes being the most and least efficient, respectively [12]. Because human cell lines contain mostly the π isozyme [32], complete conjugation of GSH with mBCl in human cell lines is often not observed, even when using incubation periods as long as 1 h and mBCl concentrations as high as 1 m*M* [12, 55]. The observed fluorescence levels, therefore, are not only dependent upon GSH concentration, but on GST activity and isozyme composition. Low GST activity also may allow a significantly high proportion of side reactions to occur with other nucleophiles such as protein sulfhydryl groups. The GST activity, protein sulfhydryl content and GSH levels and distribution, however, are *all* important factors contributing to drug resistance in the cancer cell [17]. With these factors in mind, we wished to evaluate the use of microscopy to observe the intracellular fluorescence distribution in human cancer cells and determine whether these methods can detect possible compartmentalization or elevation of GSH, GST or other sulfhydryls within cellular organelles.

Two studies have been reported which used epifluorescence microscopy to image MCB-GSH in intact isolated hepatocytes [7, 9]. In one study, a nuclear to cytoplasmic fluorescence intensity ratio (f_{nuc}/f_{cyt}) of two to three was reported in cells treated with mBCl [7]. The second study reported similar (f_{nuc}/f_{cyt}) values in isolated hepatocytes whether the cells were treated with mBCl or microinjected with MCB-GSH [9]. This latter study suggested that the increased nuclear fluorescence associated with mBC1-treated hepatocytes is more indicative of the binding and transport properties of the MCB-GSH conjugate than representative of the true intracellular distribution of GSH.

More recently, an (f_{nuc}/f_{cyt}) ratio of 0.57 has been reported in EMT-6 cells in fluorescence microscopic studies utilizing the sulfhydryl reactive agent mercury orange [51]. In this study, nuclear GSH was found to be more resistant to BSO-induced depletion than cytoplasmic GSH. The mercury orange-based method has the advantage that the product of the reaction of this dye and GSH precipitates inside the cell, thereby circumventing potential problems with diffusion and transport. However, the acetone/water staining and washing used with this method is not compatible with the study of living cells.

Other recent studies utilizing 2,3-naphthalenedicarboxaldehyde derivatization of GSH have indicated intracellular fluoresence heterogeneity of neuronal cells examined by confocal microscopy, although detailed analysis of GSH distribution was not performed [41]. All of these reports led us to examine the feasibility of using fluorescence microscopy to examine possible differences in GSH distributions in drug-resistant cell lines. Since many of the previous flow cytometric studies of human cancer cells utilized mBCl, we sought to determine whether this probe, combined with microscopic imaging techniques, could be used to measure the GSH distribution in parental, wildtype MCF-7 cells (MCF-7wt) and sublines displaying resistance to 4-hydroperoxycyclophosphamide (MCF-7hc) and adriamycin (MCF-7adr).

We report the use of epifluorescence and confocal fluorescence microscopic methods to determine relative fluorescence intensities within the nucleus and cytoplasm, as well as overall fluorescence intensities for MBCl-treated MCF-7 cells. Except for the last study cited above, confocal laser scanning microscopy has not been extensively used to quantify intracellular fluorescence distribution. Confocal microscopy provides enhanced resolution over traditional light microscopy as well as the ability to optically section through specimens. The conventional wide-field microscope accepts light from planes above and below the plane of focus and, therefore, lacks depth discrimination for three-dimensional imaging. Although out-of-focus light in epifluorescence micrographs can be substantially reduced using computational techniques, these methods require knowledge of the point spread function of the system and are computationally intensive [1].

The results of studies using both microscopic techniques indicated that the mean integrated cellular fluorescence intensities for the MCF-7 cell lines increased in the order MCF-7adr ≈ MCF-7wt < MCF-7hc. Epifluorescence measurements showed f_{nuc}/f_{cyt} values ranging from 1.3 to 1.8 for the three cell lines. Confocal images showed more evenly distributed intracellular fluorescence intensity in all cell lines with f_{nuc}/f_{cyt} values not greater than 1.1. Confocal optical sectioning also showed that MCF-7 cells grown in monolayers were typically 1–3 μm thicker in the region expected for the nucleus, thus suggesting that fluorescence from an out-of-focus plane may result in the overestimation of f_{nuc}/f_{cyt} values determined from epifluorescence images. Epifluorescence images of GSH-depleted cells still showed high levels of fluorescence, indicating significant levels of nonspecific binding of mBCl or MCB-GSH.

For all three sublines, export of the MCB-GSH conjugate was observed during the incubation period with mBCl, with the MCF-7adr displaying the most rapid efflux of conjugate.

Materials and methods

Cell lines

MCF-7wt cells were obtained from the American Type Culture Collection. MCF-7hc and MCF-7adr cells were generously supplied by Dr. Beverly Teicher (Dana-Farber Cancer Institute, Boston, Mass.). All cell lines were cultured in minimum essential medium (MEM) supplemented with 10% fetal bovine serum (FBS), 2.2 g/l sodium bicarbonate, 5 m*M* glucose, 5000 U/l penicillin and 5 mg/l streptomycin. Cells were incubated at 37 °C in an atmosphere of 95% air/5% CO_2. For microscopy experiments, 2×10^5 cells in 2 ml medium were added to Petri dishes containing a coverslip and analyses performed 3 days later when the dishes contained a total of $4–9 \times 10^5$ cells. Cell viability after mBCl treatment was checked by exclusion of trypan blue. Cells were mycoplasma free.

Materials

The fluorescent probes mBCl and mBBr were obtained from Calbiochem (La Jolla, Calif.). GSH, *N*-acetyl-L-cysteine, L-cysteine, γ-glutamylcysteine, BSO, trypsin-EDTA, Hanks's balanced salt solution (HBSS) without Mg^{2+} and Ca^{2+} salts, and Eagle's MEM were purchased from Sigma Chemical Co. (St. Louis, Mo.). FBS was purchased from Gibco (Gaithersburg, Md.). Ethanolic stock solutions of mBCl and mBBr were kept in the dark at 4 °C and analyzed quantitatively using UV spectroscopy and molar extinction coefficients provided by Calbiochem. A stock solution of 100 μ*M* MCB-GSH was prepared as previously described [9] and was analyzed quantitatively using UV spectroscopy [27]. Bimane adducts of cysteine, *N*-acetylcysteine, and γ-glutamylcysteine were synthesized by mixing equal molar quantities of the thiol and mBBr in 25m*M* HEPES, pH 7.4, for 1 h 25 °C.

GSH assays

Total GSH content (reduced and oxidized GSH) was determined by a modification of the method of Tietze [52] as described by Akerboom and Sies [2]. GSH was also determined fluorimetrically using mBBr in conjunction with HPLC. Monobromobimane reacts spontaneously with thiols to form bimane–thiol conjugates [26]. For the HPLC assay, dishes were seeded with 2×10^5 cells. After 3 days, half the dishes were used to obtain an average cell count. Cells in the remaining dishes were washed with FBS-free MEM after which 0.8 ml of this medium was added followed by 25 μl of 25 m*M* mBBr. The dishes were then placed in an incubator at 37 °C. After 60 min, the dishes were placed in liquid nitrogen. Upon thawing, the samples were deproteinized by adding equal volumes of cold perchloric acid (2 *M*) or 5% sulfosalicylic acid and centrifuged at $10\,000 \times g$ for 10 min. After neutralization of the supernatant with 5 *M* KOH, samples were filtered through a 0.22 μm filter and the total volume measured. The MCB-GSH content was determined in these samples using HPLC.

Cells were depleted of GSH by treatment with MEM containing 0.5 m*M* BSO for 36 h.

HPLC methods

MCB-GSH in cell extracts derived from mBBr- or mBCl-treated cells was quantified using a modification of an HPLC method previously reported [38] using a reverse-phase 5 μm C18 column. A binary mobile phase was used consisting of component A (18% methanol in 0.25% glacial acetic acid, pH 3.8) and component B (100% acetonitrile). The chromatographic run was initiated with 100% A for 5 min followed by a linear decrease to 70% A from 5 to 10 min. From 17 to 20 min, component A was increased linearly to 100% and remained at 100% for 30 min or until the next injection. Bimane-associated fluorescence was detected using an FD-100 filter fluorimeter (GTI/Spectra Vision, Concord, Mass.) using excitation and emission wavelengths of 350 and 470 nm, respectively. A response time of 1 s, a lamp frequency of 50 Hz, and a range of 5 or 10 were utilized. A stock solution of 100 μ*M* MCB-GSH (in 25 m*M* HEPES, pH 7.4) diluted with the appropriate amount of mobile phase component A was used to achieve injection amounts between 10 and 200 pmol MCB-GSH. Calibration graphs were constructed on a daily basis using average peak heights ($n = 2$) of the MCB-GSH peak and were found to be highly linear, with the R coefficient ranging between 0.995 and 0.9999.

Microinjection of MCB-GSH

MCB-GSH conjugate (37 m*M*, 50 m*M* HEPES, pH 7) or Cascade Blue (1 m*M*, 50 m*M* HEPES, pH 7.4) was microinjected into the cytosol of MCF-7wt cells using a Narishige micromanipulator and Nikon PLI-188 microinjector. The cells were grown on etched locator grid coverslips and maintained at 37 °C during the injections using a Nikon NP-2 microscope stage incubator.

Epifluorescence microscopy

Cells grown on coverslips were washed with 3 ml HBSS prior to staining with 0.8 ml FBS-free MEM containing 1 m*M* mBCl. The final ethanol content was < 3%. Cells were incubated for 5 or 60 min at 37 °C in an atmosphere of 95% air/5% CO_2, after which they were washed twice (60-s washes) with 2 ml HBSS. The coverslips were then placed on a microscope slide and epifluorescent images were immediately acquired.

A Zeiss Axiovert 35 microscope (Zeiss Instrument Co., Washington, DC) complete with brightfield, Normaski D/C and epifluorescence capabilities and equipped, with a cooled CCD camera (Thomson CSF model, 14 bit ADC, Photometrics, Tucson, Ariz.) was used to collect fluorescent signals. Bimane fluorescence was detected using a 415/20 nm bandpass filter, a 460 nm dichroic mirror, a 470 nm longpass barrier filter and an exposure time of 50 ms. A BG38 red suppression filter (transmission between 330 and 628 nm) and a neutral density filter (30% transmission) were also used. The × 40 objective was used in order to image up to 35 cells in one field of view. Normaski D/C images were immediately acquired after fluorescence images. Fluorescence and Normaski images were registered (if necessary) before analysis. Normaski images were used to define cellular and nuclear boundaries which were saved as graphic overlays. The graphic overlays were used in conjunction with fluorescence images to obtain integrated fluorescence intensities on a per-cell basis. To compensate for any lens aberrations or lighting anomalies during image acquisition, all fluorescence images were "shade corrected" or "flat fielded", using the procedure described by the software provided (Biovision). Briefly, "flat fielding" involves obtaining the ratio of the intensity of a blank image of the medium alone without cells to the intensity of an identical image obtained with the shutter closed. The scaling factor produced during "flat-fielding" was multiplied by the integrated cellular fluorescence intensities determined for each cell.

To avoid possible photobleaching of the GSH–bimane adduct, several consecutive fluorescence images were acquired with the same field of view and exposure times. The first two images of this series had the same integrated fluorescence intensity with successive images of reduced intensity owing to photobleaching. Only the first image in the series was used for determining integrated fluorescence intensity. Also, D/C optics, with low light intensity was used to locate the desired field of view resulting in short (50 ms) exposure times to the excitation light.

Image processing, including dark current subtraction, defining nuclear and cytosolic boundaries, the calculation of the mean pixel intensity within the nucleus and cytosol adjacent to the nucleus, and integrated fluorescence intensity per cell was performed using software (Biovision) provided by Perceptics (Knoxville, Tenn.). The f_{nuc}/f_{cyt} values were determined by dividing the average

fluorescence intensity from 40–60 pixels in the region of the cytosol adjacent to the nucleus.

Confocal microscopy

Confocal images were acquired at Meridian Instruments (Okemos, Mich.) using an Ultima scanning laser confocal microscope. Cells were grown on Nunc LabTek coverslip chambers. Cells were prepared in an identical fashion to experiments using epifluorescence microscopy using only the 5-min loading period. Coverslips were not used in order to minimize any possible physical distortion of the cells caused by the weight of the coverslip. A × 100 objective was used, thus capturing up to 5–8 cells within the field of view. Excitation of MCB-GSH fluorescence was accomplished using the UV band (351–363 nm) of an Enterprise laser. Induced fluorescence was detected using a longpass barrier filter (395 nm) and a pinhole diameter of 60 μm. For each *XY* image (*z*-slice), 360 × 360 points were collected. Typically, 18 optical slices were collected for each *z*-series using a vertical increment (*z* step) of 0.6 μm, the initial slice corresponding to the focal point at or near the cell/glass interface. Integrated cellular fluorescence intensities for 5–9 cells of each subline was measured using *z*-slices corresponding to the cell height midpoint. Images were rendered using NIH Image (version 1.56) supported by a Macintosh IIci computer.

Estimates of f_{nuc}/f_{cyt} values were obtained from *z*-slices corresponding to the cell height midpoint. In all cells, regions of interest were randomly selected and the mean and variance of the distribution of pixel fluorescence intensities within these regions were determined. If the mean and variance of fluorescence distribution was not significantly different between these randomly selected regions, value of f_{nuc}/f_{cyt} was set to 1.0 for these cells. In some of the cells, the nucleus could be observed in the confocal micrograph. In these cells, f_{nuc}/f_{cyt} values were estimated by dividing the mean fluorescence intensity from ~ 100 pixels corresponding to the center of the nuclear region by ~ 100 pixels outside this region midway to the cellular borders. The values given in Table 1 are the average f_{nuc}/f_{cyt} values for a field of cells.

Rates of GSH conjugation and export

Cells were washed with 2 ml HBBS and then treated with 0.8 ml FBS-free MEM containing 1m*M* mBCl. The dishes were immediately placed in an incubator. A 200-μl aliquot of the medium from each dish at selected times was added to 15 μl 1 *M* HCl (to quench further conjugation of GSH with mBCl) before freezing in liquid nitrogen. The rest of the medium in each dish was discarded and the cells washed twice with 2 ml HBBS. The pooled washed (4 ml) were centrifuged to remove cells (if any) and then frozen in a conventional freezer. The dishes containing the washed cells were then placed in liquid nitrogen for several minutes before storage at −20 °C.

The percentage of intracellular GSH labeled with mBCl was determined as follows. The amounts of MCB-GSH measured in the decant, wash, and cells were summed and divided by the total GSH content, as determined by HPLC analysis of mBBr-treated cells, and multiplied by 100%. Reported are the means and standard deviations from three separate experiments.

The percentage of MCB-GSH conjugate remaining in the cell after loading and washing was determined as follows. The amount of MCB-GSH measured in washed, mBCl-treated cells was divided by the sum of MCB-GSH measured in the cells, loading buffer, and pooled washes, multiplied by 100%. Reported are the means and standard deviations from three separate experiments.

Fluorescence quenching by DNA

The fluorescence of 0.5 μ*M* solutions of MCB-GSH at pH 7.4 with and without 0.8 mg/ml of calf-thymus DNA was determined on a Gilford spectrofluorimeter.

Statistics

Unpaired, two-tailed Student's *t*-tests were performed using the Statview Statistics package (Abacus Concepts, Berkeley, Calif.).

Results

GSH quantification in MCF-7 cell lines

Unlike mBCl, mBBr reacts spontaneously and rapidly with sulfhydryl groups. Upon reaction with GSH, both dyes yield the fluorescent MCB-GSH conjugate. Thiols, such as GSH, undergo complete reaction with excess mBBr in pH-neutral solutions within 5–30 min. HPLC was used to quantify MCB-GSH in mBBr-treated MCF-7 cells. At the 0.76 m*M* concentration of mBBr used in this study, we found complete labeling in 5–10 min. Cysteinyl-bimane, γ-glutamylcysteinyl-bimane, MCB-GSH, and *N*-acetylcysteinyl-bimane were well-resolved on the chromatograms of standard solutions with retention times of 6.9, 8.9, 10.5, and 13.7 min, respectively. Chromatograms of deproteinized cell extracts from mBCl- and mBBr-treated MCF-7 cells in all cases showed symmetrical peaks for MCB-GSH at a retention time of 10.5 min. Changing gradient profiles yielded identical peak shapes, indicating that MCB-GSH was not coeluting with other fluorescent species. Table 2 shows the GSH contents determined in mBBr-treated MCF-7 cells and mBBr-treated GSH stock solutions using HPLC. Table 2 also shows the GSH content of MCF-7 cells and GSH stock solutions determined by the reductase recycling method [2], which quantities total GSH (i.e. GSH + 2 × GSSG). Although the GSH content determined by the HPLC assay was slightly higher in all cell lines than the value determined by the reductase recycling assay, the differences were not statistically significant.

In order to determine whether significant GSH synthesis occurred during the mBBr loading periods used in

Table 1 Average f_{nuc}/f_{cyt} values from epifluorescence and confocal microscopy. Values are means ± SD and *n* is the number of cells analyzed (*ND* not determined)

	Epifluorescence			Confocal		
	MCF-7wt	MCF-7hc	MCF-7adr	MCF-7wt	MCF-7hc	MCF-7adr
Untreated	1.30 ± 0.27 (*n* = 30)	1.32 ± 0.24 (*n* = 50)	1.77 ± 0.30 (*n* = 49)	1.04 ± 0.03 (*n* = 7)	1.09 ± 0.001 (*n* = 5)	1.07 ± 0.09 (*n* = 6)
+ BSO	1.22 ± 0.15 (*n* = 48)	1.35 ± 0.24 (*n* = 50)	1.37 ± 0.27 (*n* = 46)	ND	ND	ND

Table 2 GSH concentrations. Values are the means ± SD for *n* separate experiments

Assay	Stock GSH[a] (μ*M*)	MCF-7wt (fmol/cell)	MCF-7hc (fmol/cell)	MCF-7adr (fmol/cell)
Reductase-recycling	20.0 ± 2.0 (*n* = 3)	14.2 ± 5.6 (*n* = 6)	56.0 ± 15 (*n* = 3)	6.4 ± 2.5 (*n* = 4)
mBBr/HPLC	20.6 ± 1.0 (*n* = 3)	20.3 ± 1.4 (*n* = 4)	65.0 ± 3.1 (*n* = 3)	8.5 ± 1.3 (*n* = 3)

[a]20.0 μ*M* GSH in 25 m*M* HEPES, pH 7.0

the present study, a 25-molar excess of mBBr (based on the expected cellular GSH content) was added to MCF-7hc cells grown in monolayers for increasing incubation periods. Using HPLC, the GSH contents for the MCF-7hc cells were 56.7 ± 5.1, 60.2 ± 4.2, and 55.6 ± 6.9 fmol/cell for incubation periods of 15, 30, and 60 min, respectively. Detection of mBBr in all chromatograms ensured that this reagent was present in excess. These results show that for MCF-7hc cells the rate of GSH synthesis was negligible during the assay period. We have found that this cell line exhibits the highest GSH synthetic rate (data not shown).

The extent of nonspecific binding by mBCl in MCF-7 cells was determined in cells depleted of GSH by treatment with BSO prior to treatment with mBCl. Treatment of the cells with 0.5 m*M* BSO for 36 h resulted in the reduction of GSH in MCF-7wt, MCF-7hc, and MCF-7adr cells by 95%, 93% and 93%, respectively, as determined using the mBBr/HPLC assay. These relatively high levels of BSO were used to ensure >90% depletion of GSH. Typically, lower BSO concentrations (50 μ*M*) often used in other studies, deplete only about 80% of the GSH in these cell lines [11, 19]. The amounts of GSH present in some BSO-treated cell lysates were below the level for accurate quantification by the reductase-recycling assay (<0.5 nmol). The presence of 0.5 m*M* BSO in the growth medium did not have a measurable effect on the rate of cell growth.

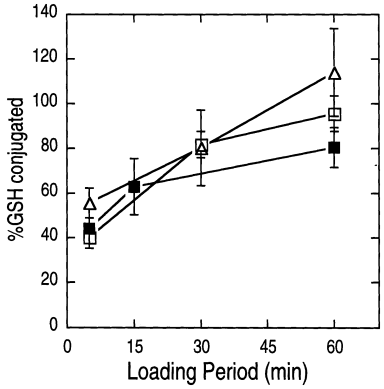

Fig. 1 Percentage of glutathione (GSH) conjugated with monochlorobimane (mBCl) in MCF-7wt (□), MCF-7hc (■), and MCF-7adr (△) cells using different loading periods. Results are given as the means ± SD from three separate experiments

Rate of GSH conjugation and MCB-GSH export

The rate of GSH conjugation with mBCl was investigated in all MCF-7 sublines. The MCB-GSH conjugate was quantified in the loading medium, washes, and cells treated with mBCl and divided by the total GSH content, as determined by HPLC analysis of mBBr-treated cells. As expected, it was found that for all MCF-7 cells, lengthening the incubation period resulted in an increase in the percentage of GSH labeled. Figure 1 shows the percentage of GSH conjugated with mBCl in MCF-7wt, MCF-7hc, and MCF-7adr cells after incubation for various times with 1m*M* mBCl. Essentially all endogenous GSH in MCF-7wt and MCF-7adr cells was conjugated after a 60-min incubation period. Although the extent of MCB-GSH formation increased with time, a significant loss of MCB-GSH occurred as a result of export of the conjugate during the loading and washing steps. MCB-GSH was quantified in aliquots of the loading medium sampled at various times. The percentages of intracellular MCB-GSH conjugate remaining after loading and washing using several loading periods are presented in Fig. 2 for all three cell lines. It was found that a 5-min loading period resulted in a 20–30% loss of MCB-GSH from all MCF-7 cells, whereas 60-min loading period resulted in losses of 42 ± 4%, 55 ± 7%, and 85 ± 3% from MCF-7wt, MCF-7hc, and MCF-7adr cells, respectively.

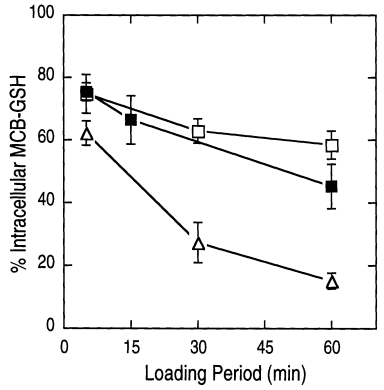

Fig. 2 Percentage of intracellular glutathione-bimane conjugate (MCB-GSH) vs. total MCB-GSH as a function of incubation period with mBCl in MCF-7wt (□), MCF-7hc (■), and MCF-7adr (△) cells. Results are given as mean ± SD from three separate experiments

Table 3 Cellular fluorescence intensity. The values are the mean cellular fluorescence intensties ± SD and *n* is the number of cells analyzed

	MCF-7wt	MCF-7hc	MCF-7adr	MCF-7wt	MCF-7hc	MCF-7adr
	60-min incubation with mBCl			5-min incubation with mBCl		
Untreated	4.7 ± 2.4 (n = 52)	7.4 ± 2.7 (n = 49)	4.4 ± 1.5 (n = 46)	13.3 ± 5.8 (n = 52)	20.8 ± 5.7 (n = 66)	5.4 ± 1.1 (n = 57)
+BSO[a]	1.5 ± 0.6 (n = 58)	2.2 ± 0.7 (n = 52)	4.1 ± 0.9 (n = 53)	4.3 ± 1.5 (n = 50)	5.2 ± 1.3 (n = 58)	3.5 ± 0.8 (n = 49)

[a]Cells were treated with 0.5 m*M* BSO for approximately 36 h before treatment with mBCl and subsequent imaging

Epifluorescence microscopy of mBCl-treated MCF-7 cells

Fluorescence and Normaski images of MCF-7 cells were acquired after incubation with 1 m*M* mBCl at 37 °C for 5 or 60 min. Under the conditions for bimane excitation and emission, fluorescence was not detected in cells not treated with mBCl; however, cells treated with mBCl were highly fluorescent. A neutral density filter and a short exposure time (i.e. 50 ms) were required to keep the signal intensity of the most fluorescent cells (i.e. MCF-7hc cells incubated for 60 min) within the linear range of the signal processor. This high level of fluorescence was expected since intracellular GSH normally exists in millimolar amounts and the MCB-GSH conjugate is highly fluorescent.

Table 3 presents mean integrated total cellular fluorescence intensities determined from epifluorescence images of untreated and BSO-treated MCF-7 cells using mBCl loading periods of 5 and 60 min. Fluorescence intensities of untreated cells increased in the order MCF-7adr ≈ MCF-7wt < MCF-7hc using 5-min loading periods and MCF-7adr < MCF-7wt < MCF7-hc using 60-min loading periods. Mean integrated fluorescence intensities of BSO-treated MCF-7wt and MCF-7hc cells were typically about 30% of untreated cells for both loading periods. Conversely, BSO-treated and untreated MCF-7adr cells showed nearly similar integrated cellular fluorescence intensities, as shown by the values in Table 3 and images shown in Fig. 3. Except for MCF-7wt and MCF-7hc cells incubated for 5 min, all fluorescence intensities of GSH-depleted MCF-7 cells were equal within experimental error.

Table 1 lists f_{nuc}/f_{cyt} values determined from epifluorescence images of untreated and GSH-depleted MCF-7 cells. Epifluorescence data showed that essentially all cells showed at least a 20% elevation in fluorescence intensity in the region of the nucleus compared to the region of the cytosol adjacent to the nucleus. However, f_{nuc}/f_{cyt} values for MCF-7adr cells were larger in untreated cells compared with cells treated with BSO. BSO-treated MCF-7adr cells, and to a lesser extent BSO-treated MCF-7hc cells, showed increased fluorescence intensity in the region of the nucleoli (Fig. 3b) after a 5-min staining with mBCl.

No difference was observed in the intracellular fluorescence intensity distributions for MCF-7wt cells treated with mBCl or microinjected with the MCB-GSH conjugate when monitored using epifluorescence microscopy. The f_{nuc}/f_{cyt} values range between 1.0 and 1.3 for cells microinjected with MCB-GSH.

Solutions of MCB-GSH with and without added calf-thymus DNA showed no difference in the fluorescence intensity.

Confocal fluorescence microscopy of mBCl-treated MCF-7 cells

The preparation of MCF-7 cells for confocal laser scanning microscopy experiments was similar to that for epifluorescence microscopy experiments. Although

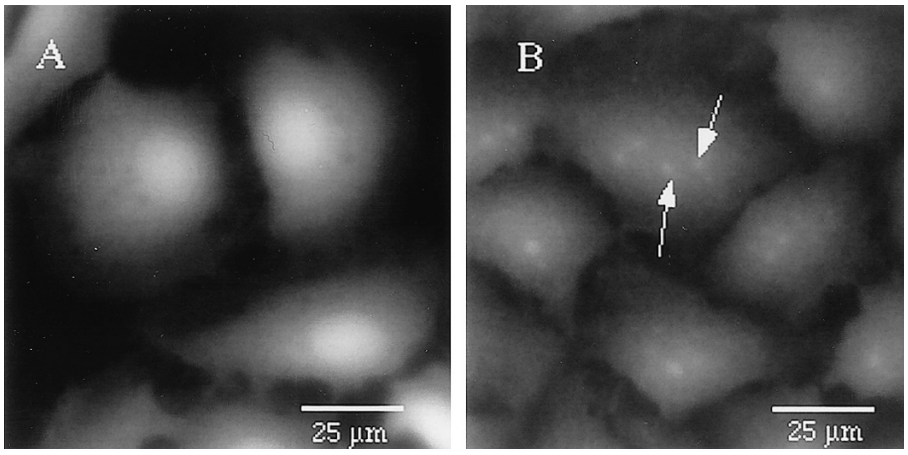

Fig. 3A,B Epifluorescence micrographs of bimane-associated fluorescence in untreated (**A**) and BSO-treated (**B**) MCF-7adr cells incubated with 1 m*M* mBCl for 5 min. Nucleoli show enhanced fluorescence intensity (*arrows*)

confocal microscopy allows optical sectioning, which yields images in the *XY* plane with little or no out-of-focus light, nuclear regions cannot be differentiated with certainty from cytosolic regions without the use of an additional fluorescent probe to visualize the nuclear membrane. This was done only for a limited number of cells. For each optical sectioning experiment, 18 images were acquired, each with the focal plane incremented along the *z*-axis by 0.6 μm (Fig. 4). Slices corresponding to the cell height midpoint were used to determine integrated cellular fluorescence intensities and to examine intracellular fluorescence intensity heterogeneity.

Although the fluorescence intensity varies from pixel to pixel in confocal images, no intracellular structures were discernible for most of the cells examined. By the criteria described in the Materials and methods section, a value for f_{nuc}/f_{cyt} was set to 1.0 for these cells.

Some cells exhibited a large region of slightly increased fluorescence intensity or a narrow ring of decreased fluorescence intensity. The size and location of this region was consistent with the expected location of the nucleus and the ring of decreased intensity was consistent with the expected size and location of the nuclear membrane (Fig. 4). Assuming this was the nucleus, 100 pixels within this region, and in the cytosolic region were randomly sampled. The mean values were used to obtain the f_{nuc}/f_{cyt} ratio for these cells. If this region did not represent the nucleus, the actual f_{nuc}/f_{cyt} ratio would be lower. The values of the f_{nuc}/f_{cyt} ratio given in Table 1 are the average for a field of cells. Figure 4 shows several optical slices taken from a *z*-series of MCF-7wt cells. Figure 4 also illustrates the typical intercellular heterogeneity encountered among mBCl-treated MCF-7 cells when examined by fluorescence microscopy.

Confocal optical sectioning is able to yield information on cell morphology. The optical sectioning results showed that most MCF-7wt and MCF-7hc cells were between 8 and 11 μm thick, whereas MCF-7adr cells were thinner, ranging from 4 to 7 μm thick. This is consistent with the fact that MCF-wt, MCF-7hc, and MCF-7adr cells possessed essentially the same cellular

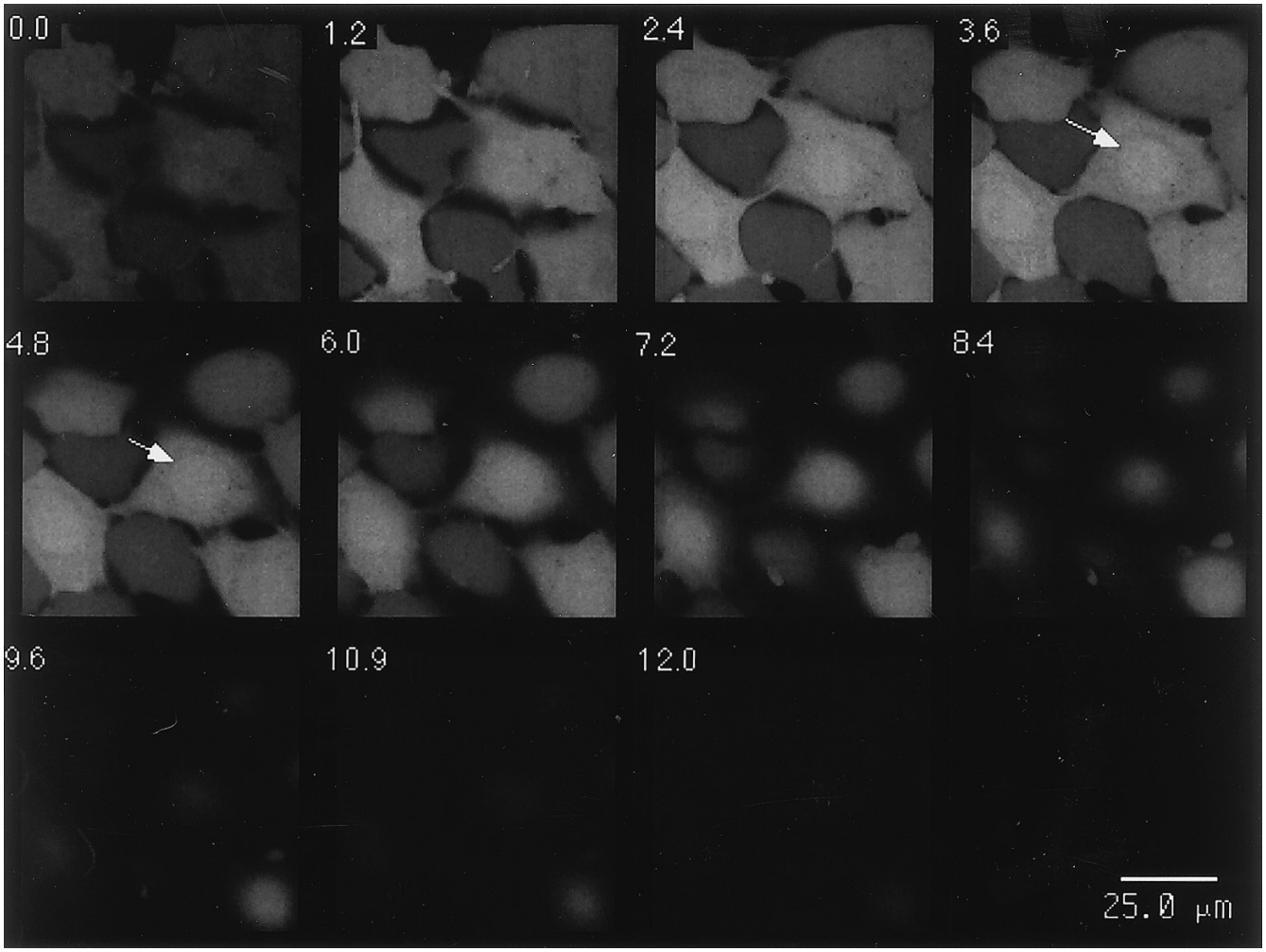

Fig. 4 Optical sections of MCF-7wt cells taken by confocal laser scanning microscopy after incubation with 1 m*M* mBCl for 5 min. The distances (in μm) along the *z*-axis from the bottom of the cells are indicated for each *XY* image

volume, even though MCF-7adr cells possessed, on average, an approximately 40% greater area than MCF-7wt and MCF-7hc cells, as determined from epifluorescence measurements (data not shown). Confocal fluorescence images of MCF-7hc and MCF-7wt cells also showed that mitotic cells (weakly adherent) could reach twice the height of nonmitotic adherent cells, i.e. 20–25 μm. There was no observed correlation between cell height, including mitotic/nonmitotic cells, and fluorescence intensity. The optical sectioning results also showed that cells of all three cell lines were about 1–3 μm thicker in the region of the nucleus.

Integrated cellular fluorescence intensities determined from epifluorescence images cannot be compared directly with the results obtained from confocal imaging. Therefore, integrated cellular fluorescence intensities for each method were normalized to MCF-7wt cells. Confocal data showed that integrated cellular fluorescence intensities for MCF-7wt, MCF-7adr, and MCF-7hc cells incubated for 5 min were in the ratio 1:0.91:2.3, respectively. These results are similar to results obtained using epifluorescence microscopy, where integrated cellular fluorescence intensities for MCF-7wt, MCF-7adr, and MCF-7hc cells incubated for 5 min were in the ratio 1:0.94:1.55, respectively.

The mean integrated cellular fluorescence intensities of cells incubated for 60 min with mBCl were corrected for nonspecific binding by subtracting the fluorescence intensity of cells depleted of GSH by BSO treatment and normalized to the MCF-7wt cell line. For a 60-min incubation period the relative mean integrated fluorescence intensities were 1:022:1.82 for MCF-7wt, MCF-7adr, and MCF-7hc cells, respectively.

Discussion

The presence of a subpopulation of drug-resistant cancer cells is thought to be a primary cause for the failure of cancer chemotherapy. Because drug-resistant cells often have elevated GSH levels and/or GSH-dependent enzymes such as GSH peroxidases and GST [36, 40], there has been a considerable amount of interest in the development of methods to quantify the interecellular GSH content in individual human cancer cells. Among the available methods, flow cytometry has been the most widely used and is capable of determining subpopulations of cells with elevated GSH levels. The GSH probe, mBCl, was developed to fluorescently label GSH in cells and is often used in conjunction with flow cytometry [46]. However, flow cytometric methods are not capable of determining the intracellular distribution of GSH in single cells, which may be of importance for understanding the GSH-associated mechanisms of drug resistance. Fluorescence microscopy methods are capable of localizing biochemical and structural components of living cells and can be used to obtain statistical information on intercellular fluorescence intensity heterogeneity if a sufficient number of cells are analyzed.

Although mBCl is often the probe of choice to fluorescently label intracellular GSH, recent studies have revealed a number of limitations to its use. One limitation is that the rate of MCB-GSH synthesis is GST isoenzyme dependent [12] which may lead to incomplete labeling of GSH [55]. The compartmentalization and availability of GSH for mBCl conjugation, i.e. mitochondrial [34] and nuclear [9] GSH, may furher influence cellular fluorescence levels. In addition, loss of the conjugate from the cell [56], nonspecific binding of mBCl [37, 56], inhibition of GST by MCB-GSH [12], and parameters such as mBCl concentration, loading period and temperature will further affect observed fluorescence levels. It is therefore essential that if steady-state levels of MCB-GSH fluorescence are to be correlated with intracelluar GSH levels for a given cell line or between different tumor cell lines the limitations of mBCl must be addressed. Therefore parameters such as mBCl concentration, loading period, and temperature must be optimized in such a way as to maximize the amount of MCB-GSH formed with minimal nonspecific binding and loss from the cell. This, in part, was the aim of the study.

All experiments described here were carried out at 37 °C in order to maintain the cells under physiological conditions during loading and to enhance the rate of conjugation. This same temperature has been used in some previous studies [10, 22, 56] but is higher than that used in others. Using a concentration of 1 m*M* mBCl in the loading buffer, we found that 95.6 ± 7.9 and 114.0 ± 15.5% of GSH was labeled with mBCl after 1 h in the MCF-7wt and MCF-7adr cells, respectively. This represents a higher degree of conjugation than previously reported, i.e. 70 ± 4 and 87 ± 3% for MCF-7wt and MCF-7adr cells, respectively, at 25 °C [12]. A higher percentage of GSH was labeled in the MCF-7adr subline than in the wildtype cells, presumably because of the higher levels of GST reported to be present in this subline [5]. No previous investigation has been reported of mBCl conjugation in the MCF-7hc subline. However, incomplete labeling in this cell line, with the highest GSH content, may be a result of inhibition of GST by the high MCB-GSH conjugate concentration [12].

We found significant levels of MCB-GSH in the extracellular medium during mBCl loading. The MCF-7adr cells showed the most rapid export of conjugate with 85% of the total MCB-GSH lost after 1 h of incubation. This rate of export is similar to the reported 87% loss of MCB-GSH in peripheral blood mononuclear cells under similar conditions [56]. However, after a 5-min loading period, we found substantially less extracellular conjugate (20–30%) than in the previous study (67%). This loss of intracellular MCB-GSH will have a significant affect on the fluorescence levels measured by microscopy or by flow cytometry.

In addition, for MCF-7 cells, this rapid export of the conjugate (even after 5 min) could affect the equilibrium concentration of GSH calculated when fluorescence intensities collected within the first 5–6 min after mBCl

introduction are extrapolated using a first-order kinetic model proposed previously [4].

It must be noted that the present results do not allow us to discriminate between active export of the MCB-GSH conjugate and the development of membrane leakiness as a result of GSH depletion. Trypan blue exclusion was maintained in mBCl- and mBBr-treated cells arguing for some retention of membrane integrity. However, the possibility that membrane changes in GSH-depleted cells allow MCB-GSH to diffuse out of the cell more easily cannot be ruled out.

The observed differences in the rate of MCB-GSH loss between the cell lines (relative rates: MCF-7wt ≤ MCF-7hc « MCF-7adr) may argue against passive diffusion out of the cell as the sole mechanism for loss of the conjugate. The rapid loss of MCB-GSH from the MCF-7adr line may be related to the presence of the *MDR*1 P-glycoprotein in this subline [14]. The results suggest that the MCB-GSH adduct may be a substrate for this efflux mechanism which is reported to play a role in efflux of hydrophobic compounds from the cell [20]. Other recent studies have implicated a non-P-glycoprotein efflux mechanism for GSH conjugates via the multidrug resistance-associated protein (MRP) [23]. We do not know if the MCF-7adr line contains MRP but an etoposide-resistant MCF-7 subline exhibits elevated levels of mRNA for MRP [49]. Although this cell line is sensitized by BSO treatment [50], as is the MCF-7adr line [29], it is unclear whether MRP is an important contributor to overall resistance.

The confocal data show that MCB-GSH fluorescence was evenly distributed in the MCF-7 cells with f_{nuc}/f_{cyt} values not greater than 1.1. These results differ from the epifluorescence measurements which showed greater fluorescence intensity in the region of the nucleus for all cell lines studied whether treated with mBCl or microinjected with the MCB-GSH conjugate (f_{nuc}/f_{cyt} ranges from 1.3 to 1.8). Our results also differed from the results obtained with isolated rat hepatocytes treated with mBCl [7] or microinjected with the MCB-GSH conjugate [9] which showed a two- to threefold increase in fluorescence associated in the region of the nucleus. It is possible that a limitation of epifluorescence microscopy, i.e. accepting light from planes above and below the plane of focus, is at least in part responsible for the larger f_{nuc}/f_{cyt} values determined from epifluorescence images than from confocal images. However, this does not explain the results obtained in previous studies [7, 9] using rat hepatocytes, because it has been reported that the region of the nucleus is actually thinner than the region occupied by the cytosol. Previous microscopic studies of EMT-6 cells did not address possible variations in subcellular fluorescence intensity resulting from differences in cell thickness [51].

It also is possible that there are differences in diffusion and/or binding of mBCl or the MCB-GSH conjugate between the nucleus and cytoplasm. Such questions may be addressed by using methods outlined recently to limit GSH–dye conjugate diffusion [51] but this method must be combined with confocal microscopic techniques.

The presence of significant fluorescence in GSH-depleted cells indicates a substantial contribution of nonspecific binding of the mBCl probe. After a 60-min incubation with mBCl, the integrated fluorescence intensity of GSH-depleted cells was similar for all three cell lines and was evenly distributed throughout the cell. This implies that all cell lines appeared to exhibit approximately the same amount of nonspecific binding. For the MCF-7wt subline, the estimated nonspecific binding was about 30% which is higher than the 17% reported previously [13]. In comparison, nonspecific binding of about 45% has been observed in the human MGH-U1 cell line after 30 min of incubation with 1m*M* mBCl [22]. Interestingly, an increased fluorescence intensity was detected in regions occupied by nucleoli in BSO-treated MCF-7adr and MCF-7hc cells in epifluorescence micrographs. The confocal data of untreated MCF-7 cells showed the region expected of the nucleus to be relatively flat. Although confocal data were not collected for BSO-treated cells, we have not previously observed changes in cellular morphology with BSO treatment using light or epifluorescence microscopy. The increased fluorescence intensity in the nucleoli may have been a result of greater nonspecific binding of the mBCl probe, or it may have reflected a pool of GSH resistant to BSO depletion.

The relative GSH contents as determined by the mBBr/HPLC assay for MCF-7wt, MCF-7adr, and MCF-7hc cells, normalized to MCF-7wt cells, were in the ratio 1:0.42:3.22 (Table 2). Integrated total fluorescence intensities for the three cell lines determined from epifluorescence and confocal data yielded ratios of 1:0.91:2.3 and 1:0.94:1.55, respectively. Even when nonspecific binding of the mBCl is not taken into account, qualitatively the fluorescence data is consistent with the actual GSH content. This is likely a result of the uniformity in the inter- and intracellular distribution in the nonspecific binding.

The elevated levels of GSH observed in the MCF-7hc subline correlated with resistance to 4-hydroperoxycyclophosphamide. In contrast, the resistant MCF-7adr subline showed lower levels of GSH relative to the MCF-7wt line. Therefore, predictions of relative drug sensitivity for the MCF-7adr based on steady-state levels of GSH alone would be in error. The combination of the elevated levels of GST in this subline relative to the others, plus a more rapid efflux of the MCB-GSH conjugate, may combine to compensate for the lower GSH levels. Research in our laboratory has indicated increased rates of GSH synthesis in the MCF-7adr line relative to MCF-7wt [18]. Similarly, based on BSO depletion rates and the higher levels of γ-glutamylcysteine synthetase activity measured in the MCF-7adr line, Batist et al. [6] concluded that the utilization of GSH in the resistant line was more rapid compared with the MCF-7wt cells. They proposed that GSH conjugate efflux may play a role in more rapid GSH depletion in the

MCF-7adr line [6]. Our results directly support their hypothesis. Together with *MDR1* and MRP-based mechanisms, these findings emphasize the need to measure the rates of GSH synthesis and depletion in drug-resistant cells as a more accurate indicator of drug resistance.

Our confocal data provide no evidence for significant heterogeneity in GSH intracellular content. Differential quenching of fluorescence may occur within the various organelles resulting in fluorescence intensity not corresponding to MCB-GSH fluorescence and the uniformity of fluorscence observed in the confocal micrographs would argue against the occurrence of significant quenching. On the other hand, the diffusion of MCB-GSH within the cell may be rapid and distinctly different from GSH resulting in a MCB-GSH distribution not reflecting normal GSH distribution. These factors cannot be ruled out and warrant further study. Young et al. have concluded that the subcellular distribution of the MCB-GSH conjugate would be more reflective of the distribution of the GST isozyme pool rather than free GSH [57]. In either case, both of these factors play an important role in drug resistance.

Acknowledgements This work was supported by NCI grant CA51229 (M.P.G.) and NIEHS Center grant ES03819 to the Johns Hopkins School of Hygiene and Public Health. The authors gratefully acknowledge Dr. Alastair Mackey for performing the microinjections and Dr. Peggy Wade and the technical staff at Meridian Instruments for access to the instrumentation and acquisition of the confocal data. We would also like to thank Drs. John Hilton, O. Michael Colvin and Susan M. Ludeman for helpful discussions and access to valuable resources in the John Hopkins Oncology Center.

References

1. Agard DA, Hiraoka Y, Shaw P, Sedat JW (1989) Fluorescence microscopy in three dimensions. Methods Cell Biol 30: 353
2. Akerboom TPM, Sies H (1981) Assay of glutathione, glutathione disulfide, and glutathione-mixed disulfides in biological samples. Methods Enzymol 77: 373
3. Asghar K, Reddy BG, Krishna G (1975) Histochemical localization of glutathione in tissues. J Histochem Cytochem 23: 774
4. Barhoumi R, Bailey R, Burghardt RC (1995) Kinetic analysis of glutathione in anchored cell with monochlorobimane. Cytometry 19: 226
5. Batist G, Tulpule A, Sinha BK, Katki AG, Myers CE, Cowan KH (1986) Overexpression of a novel anionic glutathione transferase in multidrug-resistant human breast cancer cells. J Biol Chem 261: 15544
6. Batist G, Schecter R, Woo A, Greene D, Lehnert S (1991) Glutathione depletion in human and rat multi-drug resistant breast cancer cell lines. Biochem Pharmacol 41: 631
7. Bellomo G, Vairetti M, Stivala L, Mirabelli F, Richelmi P, Orrenius S (1992) Demonstration of nuclear compartmentalization of glutathione in hepatocytes. Proc Natl Acad Sci USA 89: 4412
8. Britten RA, Green JA, Broughton C, Browning PGW, White R, Warenius HM (1991) The relationship between nuclear glutathione levels and resistance to melphalan in human ovarian tumour cells. Biochem Pharmacol 41: 647
9. Briviba K, Fraser G, Sies H, Ketterer B (1993) Distribution of the monochlorobimane-glutathione conjugate between nucleus and cytosol in isolated hepatocytes. Biochem J 294: 631
10. Burghardt RC, Barhomi R, Lewis EH, Bailey RH, Pyle KA, Clement BA, Phillips TD (1992) Patulin-induced toxicity: a vital fluorescence study. Toxicol Appl Pharmacol 112: 235
11. Chen G, Waxman DJ (1994) Role of cellular glutathione and glutathione S-transferase in the expression of alkylating agent cytotoxicity in human breast cancer cells. Biochem Pharmacol 47: 1079
12. Cook JA, Iype SN, Mitchell JB (1991) Differential specificity of monochlorobimane for isozymes of human and rodent glutathione S-transferases. Cancer Res 51: 1606
13. Cook JA, Pass HI, Iype SN, Friedman N, DeGraff W, Russo A, Mitchell JB (1991) Cellular glutathione and thiol measurements from surgically resected human lung tumor and normal lung tissue. Cancer Res 51: 4287
14. Cowan KH, Batist G, Tulpule A, Sinha BK, Myers CE (1986) Similar biochemical changes associated with multidrug resistance in human breast cancer cells and carcinogen-induced resistance to xenobiotics in rats. Proc Natl Acad Sci USA 83: 9328
15. Edgren MR (1987) Nuclear glutathione and oxygen enhancement of radiosensitivity. Int J Radiat Biol 51: 3
16. Edgren M, Révész L (1987) Compartmentalised depletion of glutathione in cells treated with buthionine sulphoximine. Br J Radiol 60: 723
17. Frei E III, Teicher B, Cucchi C, Rosowsky A, Flatow J, Kelley M, Genereux P (1988) Resistance to alkylating agents: Basic studies and therapeutic implications. In: Wooley III P, Tew K (eds) Mechanisms of drug resistance in neoplastic cells. Academic Press, New York. p 69
18. Gamcsik MP, Millis KK (1995) Measuring the rate of glutathione synthesis and degradation in drug-resistant MCF-7 cells. Proceedings of the 86th Annual Meeting of the American Association of Cancer Research, Toronto, Cadmus, Linthicum, MD, p 316
19. Gamcsik MP, Millis KK, Colvin OM (1995) Noninvasive detection of elevated glutathione levels in MCF-7 cells resistant to 4-hydroperoxycyclophosphamide. Cancer Res 55: 2012
20. Gottesman MM, Pastan I (1993) Biochemistry of multidrug resistance mediated by the multidrug transporter. Annu Rev Biochem 62: 385
21. Griffith OW, Meister A (1979) Potent and specific inhibition of glutathione synthesis by buthionine sulfoximine (S-*n*-butyl homocysteine sulfoximine). J Biol Chem 254: 7558
22. Hedley DW, Chow S (1994) Evaluation of methods for measuring cellular glutathione content using flow cytometry. Cytometry 15: 349
23. Jedlitschky G, Leier I, Buchholz U, Center M, Keppler D (1994) ATP-dependent transport of glutathione S-conjugates by the multidrug resistance-associated protein. Cancer Res 54: 4833
24. Jevtovic-Todorovic V, Guenthner TM (1992) Depletion of a discrete nuclear glutathione pool by oxidative stress, but not by buthionine sulfoximine. Biochem Pharmacol 44: 1383
25. Jocelyn PC (1975) Some properties of mitochondrial glutathione. Biochin Biophys Acta 396: 427
26. Kosower NS, Kosower EM (1987) Thiol labeling with bromobimanes. Methods Enzymol 143: 76
27. Kosower NS, Kosower EM, Newton GL, Ranny HM (1979) Bimane fluorescent labels: labeling of normal human red cells under physiological conditions. Proc Natl Acad Sci USA 76: 3382
28. Kosower EM, Pazhenshevsky B, Dodiuk H, Kanety H, Faust D (1981) Bimanes. 6. Reactive halogen derivatives of syn- and anti-1,5-diazabicyclo[3.3.0]octadienedione(9,10-dioxabimanes). J Org Chem 46: 1666
29. Kramer RA, Zakher J, Kim G (1988) Role of the glutathione redox cycle in acquired and de novo multidrug resistance. Science 241: 694

30. Lange JHM de, Schipper NW, Schuurhuis GJ, Kate TK ten, Heuningen THM van, Pinedo HM, Lankelma J, Baak JPA (1992) Quantification by laser-scan microscopy of intracellular doxorubicin distribution. Cytometry 13: 571
31. Larrauri A, Lopez P, Gomez-Lechon M-J, Castell JV (1987) A cytochemical stain for glutathione in rat hepatocytes cultured on plastic. J Histochem Cytochem 35: 271
32. Lewis AD, Forrester LM, Hayes JD, Wareing CJ, Carmichael J, Harris AL, Mooghen M, Wolf CR (1989) Glutathione S-transferase isoenzymes in human tumours and tumour derived cell lines. Br J Cancer 60: 327
33. Meister A (1991) Glutathione deficiency produced by inhibition of its synthesis, and its reversal; applications in research and therapy. Pharmacol Ther 51: 155
34. Meister A (1994) Glutathione, ascorbate, and cellular protection. Cancer Res [Suppl] 54: 1969s
35. Meredith MJ, Reed DJ (1982) Status of the mitochondrial pool of glutathione in the isolated hepatocyte. J Biol Chem 257: 3747
36. Mitchell JB, Russo A (1987) The role of glutathione in radiation and drug induced cytotoxicity. Br J Cancer 55: 96
37. Nair S, Singh SV, Krishan A (1991) Flow cytometric monitoring of glutathione content and anthracycline retention in tumor cells. Cytometry 12: 336
38. Newton GL, Dorian R, Fahey RC (1981) Analysis of biological thiols: Derivatization with monobromobimane and separation by reverse-phase high performance liquid chromatography. Anal Biochem 114: 383
39. O'Connor JE, Kimler BF, Morgan MC, Terysas KHJ (1988) A flow cytometric assay for intracellular nonprotein thiols using mercury orange. Cytometry 9: 529
40. O'Dwyer PJ, Hamilton TC, Yao KS, Tew KD, Ozols RF (1995) Modulation of glutathione and related enzymes in reversal of resistance to anticancer drugs. Hematol Oncol Clin N Am 9: 383
41. Orwar O, Fishman HA, Ziv N, Scheller RH, Zare RN (1995) Use of 2,3-naphthalenedicarboxaldehyde derivatization for single-cell analysis of glutathione by capillary electorphoresis and histochemical localization by fluorescence microscopy. Anal Chem 67: 4261
42. Ozols RF (1985) Pharmacologic reversal of drug resistance in ovarian cancer. Semin Oncol XII: 7
43. Ozols RF, Louie KG, Plowman J, Behrens BC, Fine RL, Dykes, K, Hamilton TC (1987) Enhanced melphalan cytotoxicity in human ovarian cancer *in vitro* and in tumour-bearing nude mice by buthionine sulfoximine depletion of glutathione . Biochem Pharmacol 36: 147
44. Ozols RF, O'Dwyer PJ, Hamilton TC, Young RC (1990) The role of glutathione in drug resistance. Cancer Treat Rev 17: 45
45. Poot M, Kavanagh TJ, Kang HC, Haugland RP, Rabinovitch PS (1991) Flow cytometric analysis of cell cycle-dependent changes in cell thiol level by combining a new laser dye with Hoeschst 33342. Cytometry 12: 184
46. Rice GC, Bump EA, Shrieve DL, Lee W, Kovacs M (1986) Quantitative analysis of cellular glutathione by flow cytometryutilizing monochlorobimane: some applications to radiation and drug resistance in vitro and in vivo. Cancer Res 46: 6105
47. Ross D (1988) Glutathione, free radicals and chemotherapeutic agents. Pharmacol Ther 37: 231
48. Russo A, Carmichael J, Friedman N, DeGraff W, Tochner A, Glatstein E, Mitchell JB (1986) The role of intracellular glutathione in antineoplastic chemotherapy. Int J Radiat Oncol Biol Phys 12: 1347
49. Schneider E, Horton JK, Yang C-H, Nakagawa M, Cowan KH (1994) Multidrug resistance-associated protein gene overexpression and reduced drug sensitivity of topoisomerase II in a human breast carcinoma MCF7 cell line selected for etoposide resistance. Cancer Res 54: 152
50. Schneider E, Yamazaki H, Sinha BK, Cowan KH (1995) Buthionine sulphoximine-mediated sensitisation of etoposide-resistant human breast cancer MCF7 cells overexpressing the multidrug resistance-associated protein involves increased drug accumulation. Br J Cancer 71: 738
51. Thomas M, Nicklee T, Hedley DW (1995) Differential effects of depleting agents on cytoplasmic and nuclear non-protein sulphydryls: a fluorescence image cytometry study. Br J Cancer 72: 45
52. Tietze F (1969) Enzymic method for quantitative determination of nanogram amounts of total and oxidized glutathione: Applications to mammalian blood and other tissues. Anal Biochem 27: 502
53. Tirmenstein MA, Reed DJ (1988) The glutathione status of rat kidney nuclei following administration of buthionine sulfoximine. Biochem Biophys Res Commun 155: 956
54. Treuman J, Valet G (1986) Flow-cytometric determination of glutathione alterations in vital cells by o-phthaldialdehyde. Staining Exp Cell Res 163: 518
55. Ublacker GA, Johnson JA, Siegel FL, Mulcahy RT (1991) Influence of glutathione S-transferases on cellular glutathione determination by flow cytometry using monochlorobimane. Cancer Res 51: 1783
56. Ven AJAM van der, Mier P, Peters WHM, Dolstra H, Erp PEJ van, Koopmans PP, Meer JWM van der (1994) Monochlorobimane does not selectively label glutathione in peripheral blood mononuclear cells. Anal Biochem 217: 41
57. Young PR, Connors White AL, Dzido GA (1994) Kinetic analysis of the intracellular conjugation of monochlorobimane by IC-21 murine macrophage glutathione -S-transferase. Biochim Biophys Acta 1201: 461